

Plio-Pleistocene history of Ferrar Glacier, Antarctica: Implications for climate and ice sheet stability

J.W. Staiger^{a,1}, D.R. Marchant^{a,*}, J.M. Schaefer^{b,2}, P. Oberholzer^{b,3}, J.V. Johnson^c,
A.R. Lewis^{a,d}, K.M. Swanger^a

^a Department of Earth Sciences, Boston University, Boston, MA 02215, USA

^b Institute for Isotope Geology and Mineral Resources, ETH Zürich, 8092 Zürich, Switzerland

^c Department of Computer Science, University of Montana, Missoula, MT 59812, USA

^d Byrd Polar Research Center, 135E Scott Hall, 1090 Carmack Road, Columbus OH 43210, USA

Received 15 August 2005; received in revised form 12 January 2006; accepted 16 January 2006

Available online 23 February 2006

Editor: K. Farley

Abstract

The areal distribution and elevation of glacial drifts in Vernier Valley, southern Victoria Land, are used to reconstruct the Plio-Pleistocene history of upper Ferrar Glacier. ²¹Ne cosmogenic-nuclide analyses of surface cobbles on four moraines, Ferrar 1, 2, 3, and 4, provide age control. A minimum-age estimate for Ferrar Drifts calculated by assuming zero surface erosion indicates that the oldest moraine, Ferrar 4, was deposited at least ~3400 ka. Our preferred age model, which applies a very conservative erosion rate of 5 cm Ma⁻¹ in age calculations, suggests that Ferrar 4 is ~4000 ka; Ferrar 3 is ~1200 ka; and Ferrar 2 is ~700 ka. Based on glacial geologic data, Ferrar 1 is modern; cosmogenic ages for cobbles on this moraine suggest a value for nuclide inheritance of ~50 ka.

The Ferrar drifts are most easily interpreted in terms of a progressive reduction in the ice-surface elevation of upper Ferrar Glacier during Plio-Pleistocene time. Relative to today, the surface of upper Ferrar Glacier was ~100 to 125 m higher during the Pliocene Climatic Optimum and ~50 m higher during early to mid Quaternary time. Conversely, during MIS 2, the ice-surface elevation of upper Ferrar Glacier was likely no larger than today and may have stood below modern levels.

The texture and sedimentology of all Ferrar drifts indicate that during ice recession from Vernier Valley the upper Ferrar Glacier lacked surface-melting ablation zones, even during the Pliocene Climatic Optimum. Results from a simple 2-D glaciological flow-band model demonstrate that upper Ferrar Glacier also lacked basal-melting zones during ice recession.

We show that the development of weathering pits and desert varnish on cobbles exposed at the surface of Ferrar drifts varies in accord with cosmogenic age. The mean width and depth of the largest surface pits on boulders from Ferrar drifts increases by ~10 mm Ma⁻¹ and ~6.7 mm Ma⁻¹, respectively; the maximum thickness of desert varnish on surface boulders increases by ~1.5 mm Ma⁻¹. These rates may be used to help calculate ages for dolerite-rich drifts elsewhere in the western Dry Valleys region.

* Corresponding author.

E-mail addresses: jane.staiger@dal.ca (J.W. Staiger), marchant@bu.edu (D.R. Marchant), schaefer@ldeo.columbia.edu (J.M. Schaefer), oberholzer@erdw.ethz.ch (P. Oberholzer), johnson@cs.umn.edu (J.V. Johnson), lewis.1019@osu.edu (A.R. Lewis).

¹ Present address: Department of Geology and Geophysics, National Center for Earth-surface Dynamics, University of Minnesota-Twin Cities, 310 Pillsbury Drive SE Minneapolis, MN 55455, USA.

² Present address: Lamont-Doherty Earth Observatory, Columbia University, Palisades, New York, NY 10964, USA.

³ Present address: Baugeologie und Geo-Bau-Labor, Quaderstrasse 18, 7000 Chur, Switzerland.

The general stability of the ice-surface elevation of upper Ferrar Glacier, and of the landscape in Vernier Valley, suggests minimal climatic amelioration in the upland region of the Dry Valleys during the last ~4 Ma.

© 2006 Elsevier B.V. All rights reserved.

Keywords: Antarctica; Ferrar Glacier; Pliocene; Quaternary; cosmogenic; Dry Valleys; East Antarctic Ice Sheet

1. Introduction

The areal distribution and age of glacial deposits at high altitudes (>1200 m elevation) in the western Dry Valleys region of southern Victoria Land (SVL) call for one or more expansions of the East Antarctic Ice Sheet (EAIS) during Miocene time [1]. The greatest expansion likely occurred sometime between 14.8 Ma and 12.5 Ma [1–3], when ice overtopped all but the highest peaks in the Dry Valleys [4,5]. Although general agreement exists in marine and terrestrial records for the timing of large-scale Miocene-ice expansions [2,6,7], the style of final subsequent ice retreat is debated. Did the ice sheet oscillate significantly, as did its predecessors in the Oligocene [8], and ultimately reach a minimum-ice configuration during the Pliocene [9]? Or rather, did the

ice surface lower gradually with minimal fluctuations [3]? A related question concerns coeval changes in climate [1,2]. For example, although global atmospheric temperatures during the Pliocene were several degrees warmer than at present [10], we do not yet know the magnitude of warming in SVL and the behavior of the East Antarctic Ice Sheet during this critical interval is debated [1–3,9]. Our data for ice sheet, outlet glacier, and local climate response to global Pliocene warmth presented here set a testable target for future change in a greenhouse world [11].

Our objective is to document the Plio-Pleistocene history of the Ferrar Glacier, an outlet glacier that drains Taylor Dome in SVL. Given that Taylor Dome is situated near the coast, changes in coastal storm tracks influence snow accumulation and hence the ice-

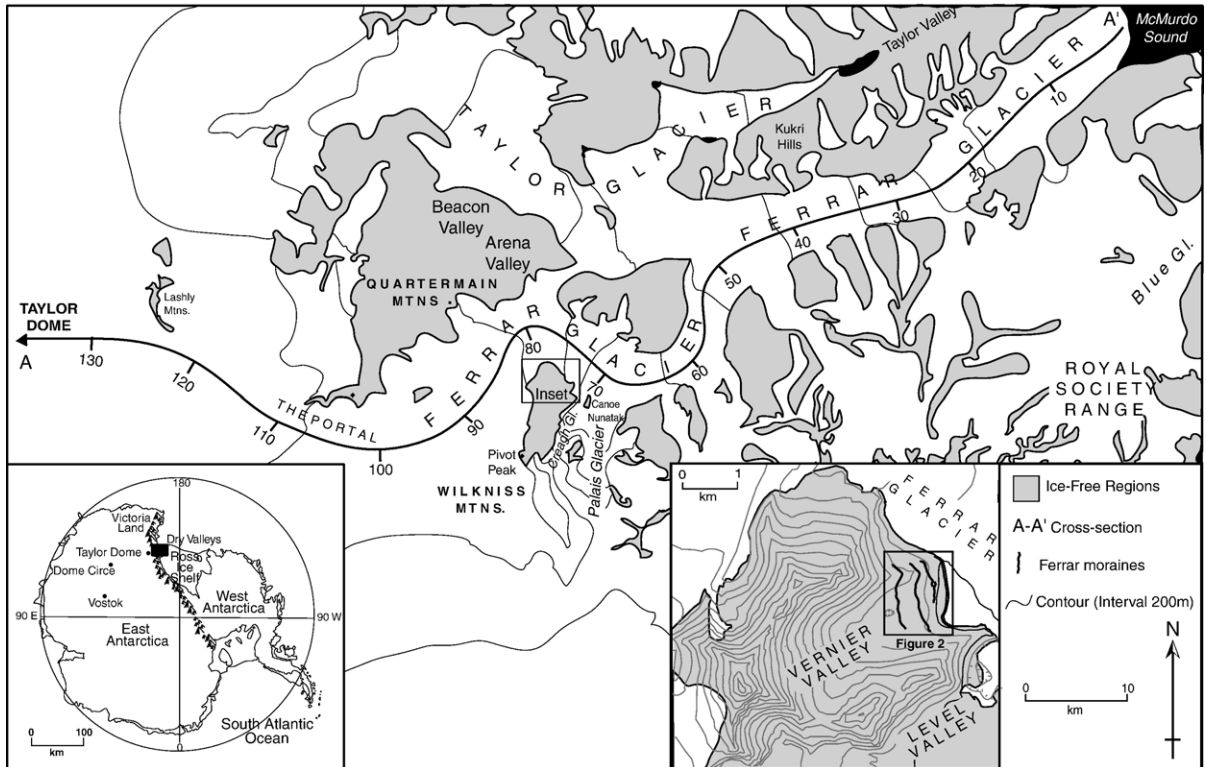


Fig. 1. Location map of the western Dry Valleys region; inset shows location of Vernier Valley in the Wilkness Mountains. Line along axis of Ferrar Glacier is measured in km. Grounding line for modern Ferrar Glacier lies at ~15 km.

surface elevation at Taylor Dome [12,13]. Only large-scale increases in the ice-surface elevation of interior East Antarctica (>100 – 200 m) are sufficient to overwhelm Taylor Dome [14]. Given this glaciological setting, the ice-surface elevation of upper Ferrar Glacier is sensitive to small-scale changes in local climate and to large-scale ice-volume fluctuations in interior East Antarctica [3,4].

1.1. Vernier Valley

Located at the inland edge of the Dry Valleys region, Vernier Valley is predominantly free of surface ice and is centered in the sandstone-and-dolerite capped Wilkniss Mountains ($\sim 77^{\circ}58'S$ and $161^{\circ}10'E$). A frozen-based lobe of Ferrar Glacier occupies the valley mouth (Fig. 1). Mean annual temperatures approach $-27^{\circ}C$. Maximum ice-surface velocities for upper Ferrar Glacier near Vernier Valley are probably ~ 14 m yr $^{-1}$ [15].

A blue-ice ablation zone occurs at the mouth of Vernier Valley. Adiabatically warmed katabatic winds descend the seaward slopes of the Wilkniss Mountains and sweep northeastward across Ferrar Glacier. These relatively warm winds increase sublimation and encourage ice flow into Vernier Valley. This flow, together with rockfall from dolerite cliffs onto Ferrar Glacier north of Vernier Valley, concentrates supraglacial debris and facilitates moraine formation at the valley mouth. Because mountain topography governs the trajectory of katabatic winds, this local blue-ice

ablation zone most probably persisted during deposition of all Ferrar drifts.

At least four Ferrar drifts lie distal and sub-parallel to the modern Ferrar Glacier in Vernier Valley (Figs. 2 and 3). A single moraine marks the upper limit of each mapped drift. To simplify terminology, we use Ferrar 2, Ferrar 3, and Ferrar 4, to represent drifts and associated moraines that crop out with increasing elevation and with increasing distance from Ferrar Glacier. We reserve Ferrar 1 drift for the weakly developed, modern moraine at the present ice margin (Fig. 3).

2. Methods

2.1. Drift characterization

Ferrar drifts were mapped based on aerial photographic interpretation and from fieldwork conducted in Vernier Valley from 1999 to 2003. Drift characteristics presented in Table 1 are based on morphologic and sedimentologic analyses of 75 soil pits, each excavated to a depth of ~ 1 m. At each soil excavation we collected a suite of soil samples, generally at 20- to 30-cm depth increments. Samples were dry-sieved in the field; the 16- to 64-mm fraction (gravel) was examined for evidence of glacial abrasion (striations, polish, molding). The <16 mm fraction was analyzed at Boston University using standard wet and dry sieving procedures in order to calculate the relative wt.% of fine gravel, sand, silt, and clay. The degree of visible staining by oxidation of iron-bearing minerals in near-surface matrix sands was gauged in the field by reference to standard Munsell color charts (e.g., [16]). Sub-samples of concentrated volcanic ash in the drifts were collected and stored separately in sealed whirl-pack bags.

2.2. Morphological analyses of surface cobbles

2.2.1. Weathering pits

In the field, we measured the size of surface-weathering pits on 150-pitted cobbles from Ferrar 2, 3, and 4 drifts (50 cobbles for each drift). We employed digital calipers, with a resolution of ± 0.03 mm. For each rock measured, we recorded the maximum width and depth of the largest weathering pit. To avoid complications associated with variable microclimates and intermittent cover by wind-drifted snow, we only measured cobbles along the tops of moraine crests.

2.2.2. Desert varnish

At Boston University, we measured the maximum thickness of desert varnish on 9 surface cobbles

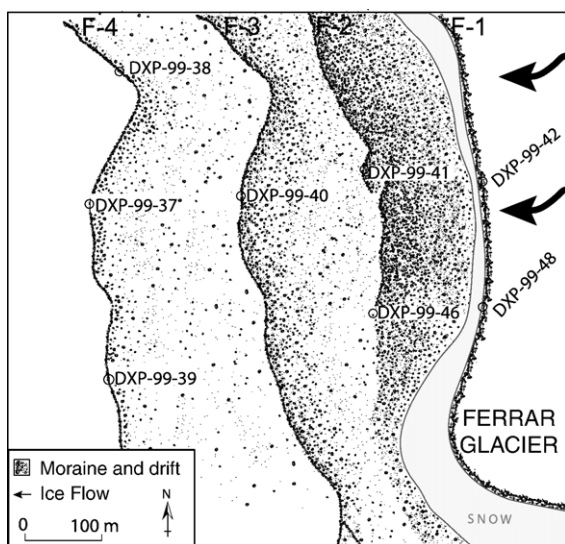


Fig. 2. Sketch map of Ferrar drifts in Vernier Valley (location shown in Fig. 1, inset); also plotted are locations for dated cosmogenic samples.

collected from the crests of Ferrar 2, 3, and 4 moraines (3 from each moraine). Rocks were sectioned and then measured using a petrographic microscope (100×); measurements are accurate to within 0.01 mm.

2.3. Geochemical analyses

2.3.1. Volcanic glass

Sub-samples of volcanic ash collected from Ferrar moraines were washed in deionized water to remove



Table 1
Physical characteristics of Ferrar drifts

Drift	(%) ^a	Grain size ^b	dol:ss ^c	Elev ^d	Height ^e	Relief ^f
Ferrar 1	98	98:1:1	80:20	1450	0	3.2
Ferrar 2	92	52:39:8	90:10	1499	49	1.8
Ferrar 3	37	76:18:6	95:5	1553	103	1.6
Ferrar 4	14	74:20:6	95:5	1576	126	1.3

^a Percentage of ground surface (excluding moraine ridges) covered by cobbles associated with Ferrar drifts; high values indicate greater drift coverage. 14% coverage for Ferrar 4 drift indicates that other than the well-defined moraine ridge, the drift is largely comprised of scattered boulders.

^b Ratios are for gravel/sand/mud.

^c Ratio of dolerite/sandstone gravel (>16 mm fraction).

^d Absolute elevation (m) of moraine ridges.

^e Maximum height (m) of moraines above adjacent Ferrar Glacier at mouth of Vernier Valley.

^f Maximum relief (m) of moraine crests.

adhering dust and fine ash. Multiple aliquots were then examined under a binocular microscope at 60×. The largest (150 to 500 μm) and densest glass shards (i.e. those not fibrous or bubble-rich) were handpicked and mounted in epoxy. The trace-element geochemistry of individually targeted glass shards was determined utilizing laser ablation (Nd:YAG, λ=213) and isotopic analyses (PQ Excell quadrupole mass spectrometer at Boston University, Department of Earth Sciences).

2.3.2. Desert varnish

Chemical analyses of transects along thin sections of desert varnish on clasts from Ferrar moraines were completed using a JEOL JXA-733 Superprobe at the Massachusetts Institute of Technology (MIT) Electron Microprobe Facility. Transects were taken from the outer rim of the weathered dolerite to the unweathered interior. Elemental concentrations were measured at 10-μm intervals.

2.4. Cosmogenic nuclide dating

A numerical chronology for Ferrar drifts comes from cosmogenic ³He and ²¹Ne analysis from pyroxene separated from eight dolerite clasts. For dating purposes,

we selected only those cobbles that were clearly and unambiguously related to moraine deposition: at each sample site we focused on collecting the uppermost cobble that capped a vertical sequence of stacked and/or perched cobbles. This practice ensured that the clasts measured were not be reworked from underlying deposits.

2.4.1. Mineral separation and gas extraction

Pyroxene aliquots were separated by magnetic and density separation and handpicking. Typical sample weights were about 20 mg.

Noble gas analyses were carried out at the Department of Earth Sciences at ETH Zürich, using a non-commercial, all-metal magnetic sector mass-spectrometer (90°, 210 mm radius) equipped with a modified Baur–Signer ion source [17] whose sensitivity is essentially constant over the pressure range relevant for this work. A stepwise heating procedure was applied in order to separate the cosmogenic gas fraction from nucleogenic or trapped gases [18]. All ³He are assumed to be cosmogenic. To calculate the concentrations of cosmogenic ²¹Ne, ²⁰Ne was assumed to be entirely atmospheric, and an atmospheric ²¹Ne/²⁰Ne ratio of 0.002959 was used (see also below and online supplement).

2.4.2. Production rates

We use the sea level, high latitude production rate value of 115 at g⁻¹ yr⁻¹ for ³He [19]. For ²¹Ne we used the elemental production rate from Si of 42.5 at g⁻¹ yr⁻¹ [20], together with the theoretically derived production rates from Mg of 185 at g⁻¹ yr⁻¹, and from Al of 55 at g⁻¹ yr⁻¹ [18,21]. Note that the modeled production from Mg contributes typically more than 50% of the total ³He production in pyroxene. These values combined with the chemical composition of the pyroxene separates yield the sea level/high-latitude production rates (see online supplement). These values are scaled to the elevation of the sampling site following the procedure of Stone [22], which takes the sea level air pressure of 989 hPa in Antarctica into account (instead of 1013 hPa for standard atmosphere). Please refer to the

Fig. 3. (a) Modern moraine (Ferrar 1) along the margin of Ferrar Glacier at the mouth of Vernier Valley. View is toward the south. (b) Sample DXP-99-40 (Ferrar 3) dated at 1100±60 ka (uncorrected ²¹Ne age). The boulder has split into several pieces, some of which occur around the base of the “core boulder” shown here. (c) Sample DXP-99-37 (Ferrar 4) dated at 1430±90 ka (uncorrected ²¹Ne age). Ken Tonka for scale. Note the large boulder in center background that shows evidence for loss of thick surface slabs (each up to 20-cm thick), leaving spalled fragments encircling a weathered dolerite core. (d) Outer limit of Ferrar 4 drift; in left foreground, note typical “puzzle-rock” formed by in situ fracture. Rock fragments surrounding this boulder can be pieced together, forming a larger core boulder (see text). The line that wraps around the bedrock rise in the background is the outer limit of Ferrar 4 drift (view is to the north). (e) DXP-99-48 (Ferrar 1) dated at 31±2 ka (uncorrected ³He age). (f) DXP-99-41 (Ferrar 2) dated at 670±60 ka (uncorrected ²¹Ne age). (g) DXP-99-38 (Ferrar 4) dated at 1660±180 ka (uncorrected ²¹Ne age). (h) DXP-99-39 (Ferrar 4) dated at 3390±190 ka (uncorrected ²¹Ne age). Note progressive increase in width and depth of pitting in panels (e)–(h).

Table 2
Cosmogenic noble gas data for Ferrar drifts

Drift	Sample	<i>a-b-c</i> axes (cm) ^a	Altitude (m)	³ He (10 ⁸ at./g)	²¹ Ne (10 ⁷ at./g)	Minimum ³ He age (ka)	Minimum ²¹ Ne age (ka)	²¹ Ne-age (ka) ^b 5 cm/Ma	²¹ Ne-age (ka) ^c of 10 cm/Ma	Max erosion rate (cm/Ma)
F-1	DXP-99-42	32-22-20	1420	0.114±0.005	0.530±0.097	22±1	51±9	51	51	1080
	DXP-99-48	50-40-15	1400	0.160±0.011	0.899±1.497	31±2				665
F-2	DXP-99-41	40-30-20	1480	3.165±0.153	8.060±0.663	570±28	670±60	690	710	82
	DXP-99-46	110-75-60	1510	(0.149±0.014)	3.177±0.231	(26±0.3)	260±20	260	270	213
F-3	DXP-99-40	125-65-60	1510	(0.607±0.054)	14.608±0.758	(110±10)	1100±60	1160	1230	50
F-4	DXP-99-37	135-55-50	1550	9.932±0.253	18.993±1.253	1690±40	1430±90	1530	1660	39
	DXP-99-38	60-30-20	1550	9.734±0.320	19.186±2.064	1660±60	1660±180	1800	1980	33
	DXP-99-39-1	45-20-15	1480	19.809±0.636	37.528±4.005	3590±120	3270±350	3880	4960	17
	DXP-99-39-2	45-20-15	1480	20.010±1.099	38.974±2.196	3630±200	3390±190	4060	5280	16

Given 2σ uncertainties include counting statistics, variations in the sensitivity, and mass discrimination uncertainty of the mass spectrometer. Uncertainties in calibration gas concentrations are not included but should be less than 3%. Aluminum foil process blanks yield negligible ³He blanks and neon blanks of atmospheric isotope composition.

For production rate systematics, see Supplementary Table A1 in the Appendix. For ³He, we used sea level/high-latitude values of 115 at./(g*yr) [47]. For ²¹Ne, we used the following sea level/high-latitude elemental production rate values: $P_{21}(\text{Si})=42.5$ at./(g*yr); $P_{21}(\text{Mg})=185$ at./(g*yr); $P_{21}(\text{Al})=51$ at./(g*yr) [18,37]. We applied the production rate scaling procedure given in Kober et al. [21], taking into account the low air pressure in Antarctica. No correction for sample thickness was applied, since processed samples were thin (<1 cm). Note that the application of other production rate values and scaling procedures, which would yield only slightly different exposure ages, would not affect the main conclusions drawn from this data set.

The minimum ages are calculated assuming zero erosion. To give a feeling for the sensitivity of the exposure ages for the process of erosion, we give all ²¹Ne-ages including a steady erosion rate of 5 cm Ma⁻¹ as well as 10 cm Ma⁻¹ (see also Fig. 6).

Maximum erosion rates are calculated from the measured cosmogenic ³He and ²¹Ne concentrations assuming infinite exposure time. For both erosion calculations, we used an attenuation length value of 155 g/cm².

The two young ³He ages for DXP-99-46 and DXP-99-40 are excluded as outliers. Discussing the reason for the too young He-ages is beyond the scope of this paper (see also text). Various studies have demonstrated that pyroxene generally retains cosmogenic He in Antarctica over time-scales of million of years [34–37].

^a Size of *a-b-c* axes (measured in cm) for whole rock prior to sampling.

^b Ne-age based on an assumed erosion rate of 5 cm Ma⁻¹, which is the lowest erosion rate published in [18].

^c Ne-age based on an assumed erosion rate of 10 cm Ma⁻¹, which is close to the lowest maximum erosion rate in this data set.

online supplement for more details on production rates. For analytical details, see Table 2.

2.5. Glaciological modeling

We modeled the basal thermal regime of the Ferrar Glacier for a suite of input parameters including atmospheric temperature and accumulation rate. In order to determine the thermal regime (melted vs. frozen) at the base of the glacier, the partial differential equation describing the temperature field of the glacier must be solved [23]. The assumptions used, and the development of the steady state solution are given in the online supplement. Our approach closely follows that cited in Hooke [24] and originally developed in Budd et al. [25].

3. Results

3.1. Ferrar drifts

The maximum elevation for Ferrar drifts above the modern Ferrar Glacier at the mouth of Vernier Valley is as follows: ~50 m for Ferrar 2, ~100 m for Ferrar 3, and ~125 m for Ferrar 4 (Table 1).

Each Ferrar drift and associated moraine is clast-supported and composed of $\geq 80\%$ Ferrar Dolerite (Table 1). Clasts at the ground surface range in size from gravel to boulders, with the frequency of large boulders generally decreasing from Ferrar 2 to Ferrar 4. In the subsurface, quartz sand and weathered dolerite grus occupy most pore space between adjacent clasts. The overall grain size and texture of Ferrar drifts is analogous to deposits of rockfall origin in the western Dry Valleys region [1] and to moraines deposited from cold-based ice in nearby Arena Valley [16,26,27].

Each of the moraines is sharp crested, ranging in height from 1 to 4 m; below the loose collection of stacked cobbles and boulders at the ground surface, the sandy matrix fraction includes concentrated layers of fine-grained (<2 mm) volcanic glass.

As noted above, surface cobbles display a gradual decrease in overall grain size with increasing distance (age) from the modern Ferrar Glacier. The clasts that comprise the outermost (oldest) moraine include a relatively high proportion of small cobbles; each of these small cobbles is commonly arrayed around a central core boulder and is demonstrably related to the in situ fracture and breakdown of the central boulder, e.g., Fig. 3b–d). For the younger moraines, i.e., Ferrar 2 and Ferrar 1 (see Numerical chronology), there is little

evidence for this type of in situ splitting and fracture of surface cobbles.

The intensity of visible near-surface oxidation in the sand-sized (<2 mm) fraction of all Ferrar drifts is generally quite low, but this value changes across drift boundaries: no oxidation is observed in Ferrar 1 drift; limited oxidation occurs in the upper 10 cm of Ferrar 2 drift, and; minor oxidation occurs in the upper 15 cm of Ferrar 3 and 4 drifts. Otherwise, soils show little visible change across drift boundaries. None of the clasts in Ferrar drifts show striations, molding, polish and/or other textural evidence for glacial erosion.

Soil excavations show that Ferrar 3 and 4 drifts rest directly on undisturbed sandstone bedrock, oxidized colluvium, or silt-rich till. Willenbring [27] correlated the silt-rich till underlying Ferrar 4 drift with the Sessrumnir till [2] based on reconstructed ice-flow directions, clast and matrix lithology, and weathering stage. The Sessrumnir till is associated with expansion of wet-based alpine glaciers during middle Miocene time [1–3,27]. Bedrock striations in association with this silt-rich till (Sesrumnir equivalent) show that ice flow was to the northeast, down the axis of Vernier Valley. This flow direction contrasts sharply with reconstructed ice flow during deposition of all Ferrar drifts, during which time Ferrar Glacier advanced southward into Vernier Valley.

3.1.1. Glass shard morphology and chemistry

Ferrar 2, 3, and 4 moraines each contain a chemically distinct and little-abraded component of concentrated, vitric basaltic ash. This ash is loose and unconsolidated; it filters through openwork gravel and loose sands during excavation of soil pits. Shards from all moraines show similar morphologic characteristics and average from 0.5 mm to 0.75 mm in length. When examined at 60 \times magnification, the majority of glass shards display delicate spires and intact bubble vesicles; Pele's hair and Pele's tears are two common glass morphologies. Glass shards show no obvious evidence for hydration and/or partial alteration to clay minerals.

ICP–MS analyses of volcanic ash in Ferrar drifts (Fig. 4) show that the trace-element geochemistry of glass shards appears chemically uniform within individual drifts, but differs among drifts. This suggests that the ash deposits were not mixed and/or reworked after initial deposition. Geochemical analyses that show the Rare Earth Element (REE) pattern for glass shards suggests that the ashes likely came from repeated eruptions at a single (or multiple closely spaced) source (s), most likely within the nearby Erebus volcanic province (<50–100 km distant) [1–3,28,29], although

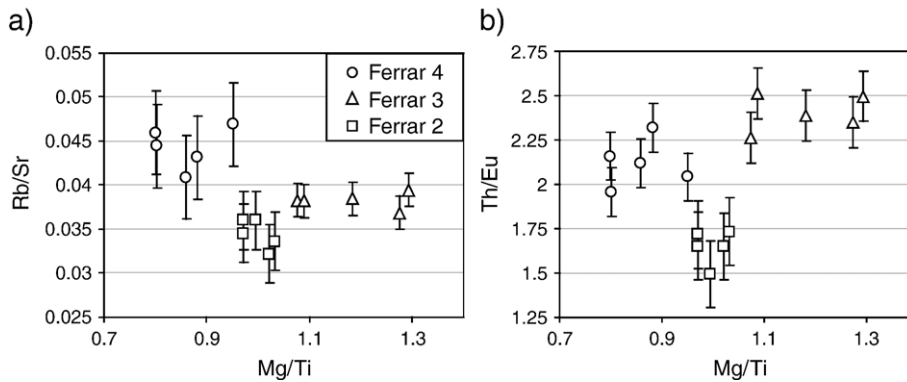


Fig. 4. (a, b) Geochemical characterization of individual volcanic glass shards within Ferrar 2, 3 and 4 drifts using trace-element data determined by LA–ICP–MS. Rb/Sr, Th/Eu and Mg/Ti were chosen for their high discriminating power. Variation bars plot ± 2 S.D. Each analysis is of a separate glass shard. Results show that each moraine contains a chemically distinct volcanic ash.

we cannot pinpoint that source (see online supplement for REE data). Our suggested history for concentrated volcanic ash in Ferrar drifts involves initial deposition onto Ferrar Glacier ice, followed thereafter by supraglacial (perhaps englacial) transport to evolving ice-marginal moraines (e.g. [27,29]). This emplacement mechanism differs from that for dated ash in nearby Beacon Valley [30], where ashfall up to 8.1 Ma fell directly into open thermal contraction cracks in ancient till [31].

3.1.2. Surface-weathering characteristics

The size of the largest weathering pit on dolerite clasts atop Ferrar drifts increases with drift age (Fig. 5). Where present, the largest pits on surface clasts increase from an average of 8 mm wide and 3.7 mm deep for Ferrar 2 drift to 32 mm wide and 24 mm deep for Ferrar 4 drift. Variance in pit measurements also increases from Ferrar 2 to Ferrar 4. Increasing variance as a function of drift age (see Numerical chronology) is expected and reflects progressive evolution and development of new pits and intermittent exposure of fresh rock surfaces arising from rock displacement and/or fracture associated with thermal expansion and contraction (e.g., [32], and references therein) (Fig. 3).

The maximum thickness of desert varnish measured for cobbles exposed on moraine crests also shows a near-linear trend with age. The results show that the thickness of desert varnish varies considerably across individual rock surfaces, but that it reaches a local maximum in rock depressions protected from wind scour. The maximum thickness of varnish on exposed cobbles shows a predictable increase from Ferrar 1 to Ferrar 4 drift (Fig. 5). These data, along with our absolute chronology for moraine deposition provided below, suggest that the rate at which varnish thickens in

our sample population is $\sim 1.5 \text{ mm Ma}^{-1}$. This value is greater than that documented by Weed and Ackert [33] and Weed and Norton [34] who measured the thickness of siliceous crust on sandstone boulders in nearby Arena Valley. Their results suggest a maximum varnish thickness of $\sim 100 \mu\text{m}$ for surface boulders later dated with cosmogenic He-3 [26] to $\sim 2.2 \text{ Ma}$. Microprobe analyses along a transect across the desert varnish on one cobble from Ferrar 4 shows chemical variation in the varnish; particularly notable is a decrease in the concentration (wt.%) of SO_4 and Cl from the rock surface inward (online supplement).

Isolated remnants of desert varnish occur on the surface of otherwise relatively “varnish-free” cobbles atop Ferrar 3 and 4 drifts. The remnants rise 4 to 5 mm above rock surfaces; micro-fractures occur at the base of most varnish remnants. The impression is that varnish may repeatedly flake off, leaving behind small, relatively intact remnants. We did not include measurements of these varnish remnants in data plotted in Fig. 5, but field data show that they are almost always ~ 4 to 5 mm thick. This value may represent a maximum threshold thickness for varnish on Ferrar Dolerite in the current climate.

Taken together, the measured changes in maximum varnish thickness and in the size of surface-weathering pits across Ferrar drifts reveal a relative chronology, with drift ages increasing from Ferrar 1 to Ferrar 4.

3.2. Numerical chronology

3.2.1. Cosmogenic dating

The cosmogenic ^3He and ^{21}Ne ages for Ferrar drifts are given in Table 2. Production rate systematics are presented in the online supplement. Some variation in cosmogenic ages for Ferrar drifts exists. In general,

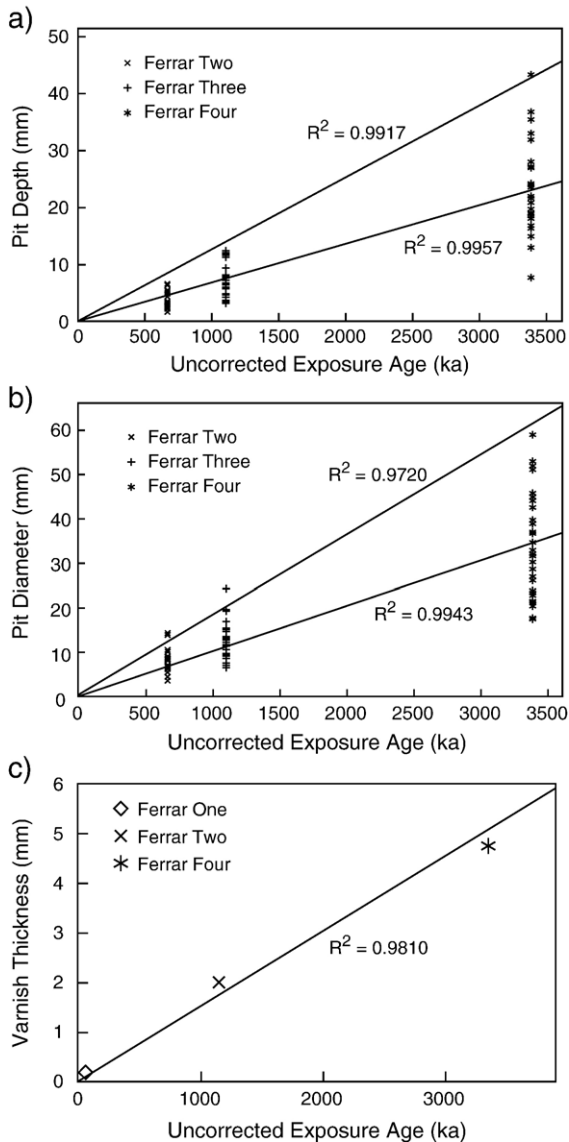


Fig. 5. (a, b) The maximum depth and width of weathering pits on cobbles of Ferrar dolerite exposed on Ferrar moraines plotted as a function of exposure age (uncorrected ages); see text for details. Lower trendline with r^2 values were determined from mean values; upper trendline from maximum values (rates reported in the text are for mean values). Note that variance in measurements increases with exposure age (see text). c. maximum thickness of desert varnish on Ferrar moraines plotted against exposure age (uncorrected ages).

the ^3He and ^{21}Ne ages agree well for samples DXP-99-41, -37, -38, -39-1, and -39-2 within uncertainties. The slight differences between the ^3He - and the ^{21}Ne -ages in these samples might be due to the uncertainty in the elemental production rate of ^{21}Ne from Mg. The production from Mg typically contributes more than 50% to the total ^{21}Ne production from pyroxene, but

is based on theoretical calculations only [18,21]. Samples DXP-99-46 and DXP-99-40 show significantly younger ^3He -ages than ^{21}Ne -ages. Discussing the reason for the young He-ages is beyond the scope of this paper. Various studies report evidence that pyroxene generally retains cosmogenic He in Antarctica over time-scales of million of years [18,35–37]. However, a recent study by Oberholzer reports systematically younger ^3He than ^{21}Ne ages from pyroxene [38]. This age discrepancy could be due to remaining plagioclase in the pyroxene separates, which can be very challenging to optically identify in the Ferrar Dolerite lithology. Since plagioclase retains about 50–70% of the cosmogenic ^{21}Ne but hardly any cosmogenic ^3He [37], this would explain the observed age differences. Additional mineralogic and crystallographic investigations are needed to understand better this important problem. Given this, we focus on the chronology provided by ^{21}Ne cosmogenic-nuclide analyses. All neon isotope data points are consistent with the two-component mixture line for cosmogenic neon isotopes from pyroxene of $(^{22}\text{Ne}/^{20}\text{Ne}) = 1.07 * (^{21}\text{Ne}/^{20}\text{Ne}) + 0.1$ [18], i.e. the data indicate a two-component mixture between cosmogenic and atmospheric neon (see Supplementary Data in the Appendix).

The cosmogenic ^{21}Ne chronology (and ^3He chronology) (Table 2) is consistent with our relative chronology. If we assume zero surface erosion, an invalid assumption based on our surface-weathering studies, and focus on the oldest results from ^{21}Ne analyses (see justification in Discussion), then the data show that the *minimum* ages are 670 ± 60 ka for Ferrar 2, 1100 ± 60 ka for Ferrar 3, and 3390 ± 190 ka for Ferrar 4.

In an effort to estimate the potential effect of nuclide inheritance on cosmogenic ages presented here, we measured the inventory of two control samples from the modern Ferrar 1 moraine (DXP-99-42 and DXP-99-48). The nuclide inventory in these samples includes (1) those that may have accumulated during prior exposure on cliff walls and (2) those that may have accumulated during supraglacial transport to Vernier Valley, as well as potential nucleogenic or inherited noble gases. The ^3He and cosmogenic ^{21}Ne concentrations of these test samples therefore reflect a maximum estimate for the pre-exposure signal. Results show that nuclide inheritance is relatively minor (Table 2), but that its value varies slightly among the two samples measured. The measured ^{21}Ne excess over air in DXP-99-42 corresponds to an exposure period of 51 ± 9 ka; ^3He ages for this sample and for DXP-99-48, also on Ferrar 1, are 22 ± 1 ka and 31 ± 2 ka, respectively (Table 2). The

higher ^{21}Ne than ^3He -age derived from sample DXP-99-42 again might be explained by remaining plagioclase in the pyroxene separate (see above). To be conservative, we use the measured ^{21}Ne excess over air as our proxy for prior exposure; i.e., the ^{21}Ne age of 51 ka. It is not possible to discern whether cosmogenic nuclides in these samples originated from prior exposure at the bedrock source, accumulation during glacial transport, or from some combination of these factors. Given our test results however, exposure ages would only be reduced by 2% to 4% for the Ferrar 4 samples, ~5% for the Ferrar 3 sample, and ~12% for the Ferrar 2 samples. These small corrections do not change the main conclusions of this paper.

4. Discussion

4.1. Erosion rates: implications for cosmogenic ages

Inspection of Table 2 reveals that surface cobbles on individual moraines vary in their concentration of cosmogenic nuclides. The result being that ages occasionally appear inconsistent. The measured variance in nuclide inventory is greatest for cobbles on Ferrar 4 drift. Given the geomorphic evidence for rock erosion presented above, and given that this erosion arises from both presumed steady-state pit development (Fig. 5) and from the larger effects of intermittent spalling and thermal fracture (Fig. 3), this variance is expected; in addition, the variance is likely to be greatest for boulders on the oldest moraines, which have had the greatest exposure duration and thus have had the highest potential for experiencing some combination of intermittent rock fracture, turn-over, and/or burial beneath thick snow banks. Field observations show that clasts at the surface of Ferrar 3 drift, and particularly on Ferrar 4 drift, show the greatest scatter in size, with surface clasts ranging from large boulders >2 m in diameter to small cobbles <20 cm in diameter. Commonly, the smallest cobbles are arrayed around, or superposed on, a larger core boulder (Fig. 3). The implication is that the small clasts have spalled off larger core fragments. In many cases, these fragments can be pieced together to create a “puzzle rock” (Fig. 3c, d). However, only the outer (spalled) rims of these puzzle rocks contain the full nuclide inventory; the cores, exposed after slabs up to 20 cm thick have slid off, will display relatively low nuclide inventories. Furthermore, many of these core boulders display relatively low numbers of weathering pits; those that do exist are anomalously small and shallow compared to those that occur on the spalled

fragments. For these reasons, we contend that the best age assessment is obtained by using the oldest dated clast on each individual moraine crest. Commonly, this clast will be one of the smallest at the ground surface. As an example, we note that sample DXP-99-39 (our oldest dated clast) is rather small, with a , b , and c axes equal to 45 cm, 20 cm and 15 cm, respectively (Table 2). This clast is one of several small fragments that appear to have spalled off a larger, nearby core boulder sometime after moraine deposition.

To assess better the absolute age of Ferrar drifts, we recalculated cosmogenic ages for a variety of erosion rates (Fig. 6). Published erosion rates for the Dry Valleys are among the lowest on Earth, ranging from ~0.05 m Ma^{-1} to ~1.00 m Ma^{-1} [18,35,37,39–41]. We also calculated maximum erosion rates from the cosmogenic nuclide inventory for all samples assuming infinite exposure. DXP-99-39, the sample with the highest cosmogenic inventory, yields a maximum erosion rate of 14 cm Ma^{-1} , consistent with very low maximum erosion rate values from dolerite surfaces in the Dry Valleys [18,42]. Although the data permit a variety of erosion rates, we consider an erosion rate of 5 cm Ma^{-1} as a reasonable and very conservative assumption; this is the lowest erosion rate

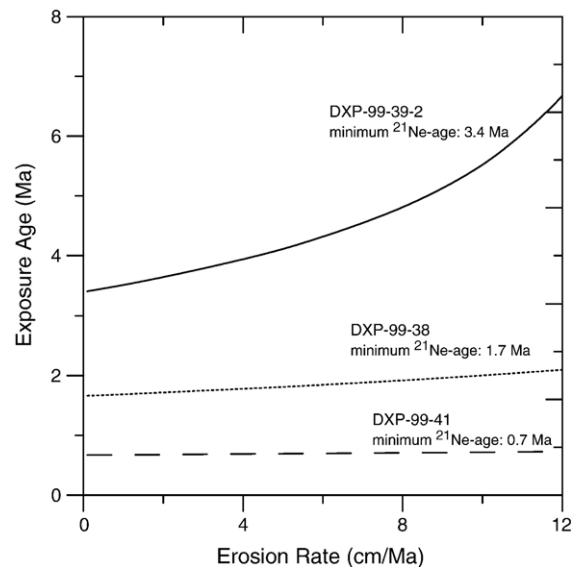


Fig. 6. Nominal ^{21}Ne -exposure age as a function of erosion for three selected Vernier Valley samples: The oldest sample in the data set, DXP-99-39-2, as well as DXP-99-38 and DXP-99-41. We used the attenuation length $\rho=155 \text{ g/cm}^2$; for production rate see online supplement. This plot illustrates that old exposure-ages are much more sensitive to even low erosion rates than young exposure ages.

reported for moraines in the western Dry Valleys region [41]. Ages calculated with this erosion rate represent our preferred age model for Ferrar drifts (Table 2). Given this erosion rate, Ferrar 4 is ~ 4060 ka, Ferrar 3 is ~ 1160 ka, and Ferrar 2 is ~ 690 ka. Also shown in Table 2 are cosmogenic ages assuming zero erosion and for a steady-state erosion rate of 10 cm Ma^{-1} . The sensitivity of our exposure ages to the process of steady state erosion is plotted in Fig. 6. As will be noted, the ages for the oldest samples are highly dependent on erosion rate. If the erosion rate exceeded 5 cm Ma^{-1} , a reasonable possibility given available data, then the values in our preferred age model reported here could vastly underestimate the true depositional age for Ferrar 3 and 4 drifts. Such a change in moraine age, however, would not affect the main conclusions of this paper.

4.2. Glacial history of upper Ferrar Glacier

4.2.1. General considerations

The overall pattern of Ferrar drifts in lower Vernier Valley, along with our relative and numerical drift chronologies afforded by surface-weathering characteristics and exposure-age data, imply progressive recession of a peripheral lobe of Ferrar Glacier from central to lower Vernier Valley. These data do not preclude with certainty that Ferrar Glacier fluctuated during its overall retreat from Vernier Valley. But, given the strong katabatic winds that develop there, any significant advance/retreat of Ferrar Glacier during Plio-Pleistocene time would likely have resulted in a discernable drift and/or moraine ridge in Vernier Valley. Accordingly, we conclude that a major fluctuation of Ferrar Glacier in Vernier Valley subsequent to the deposition of Ferrar 4 drift is highly unlikely.

4.2.2. Ice sheet retreat from middle Miocene ice expansion

Vernier Valley apparently lacks drifts from Ferrar Glacier that record initial recession from the ice sheet build up that occurred between 14.8 Ma and 12.5 Ma [1,5]. As one possible explanation, we suggest that during initial recession (commencing by at least ~ 12.5 Ma [1,5]) northeast flowing ice may have flowed out of Vernier Valley, merging with an ancestral Ferrar Glacier at the valley mouth. Such an ice configuration would have impeded moraine deposition at the mouth of Vernier Valley (e.g., [1–3]). Alternatively, the “missing moraine record” (essentially from ~ 12.5 Ma to ~ 4 Ma) could reflect an absence of suitable rockfall onto Ferrar Glacier and/or a higher

rate of surface erosion for mapped Ferrar drifts (e.g., pushing our numerical chronology for Ferrar 4 back into mid to late Miocene time, e.g., Fig. 6). We favor some combination of the first two options, and emphasize that drifts of the type mapped here could only form once Vernier Valley became largely free of ice and once suitable nunataks with dolerite bedrock emerged from beneath waning ice upstream of Vernier Valley. Erosion rates significantly greater than ~ 5 to 10 cm Ma^{-1} are inconsistent with regional geomorphic studies in the western Dry Valleys region [39,41,42]. In any case, the moraine record from Vernier Valley shows that by ~ 4 Ma the ice-surface elevation of upper Ferrar Glacier was within 125 m of its current elevation (assuming negligible surface uplift [41,43]), and that subsequent fluctuations were relatively minor.

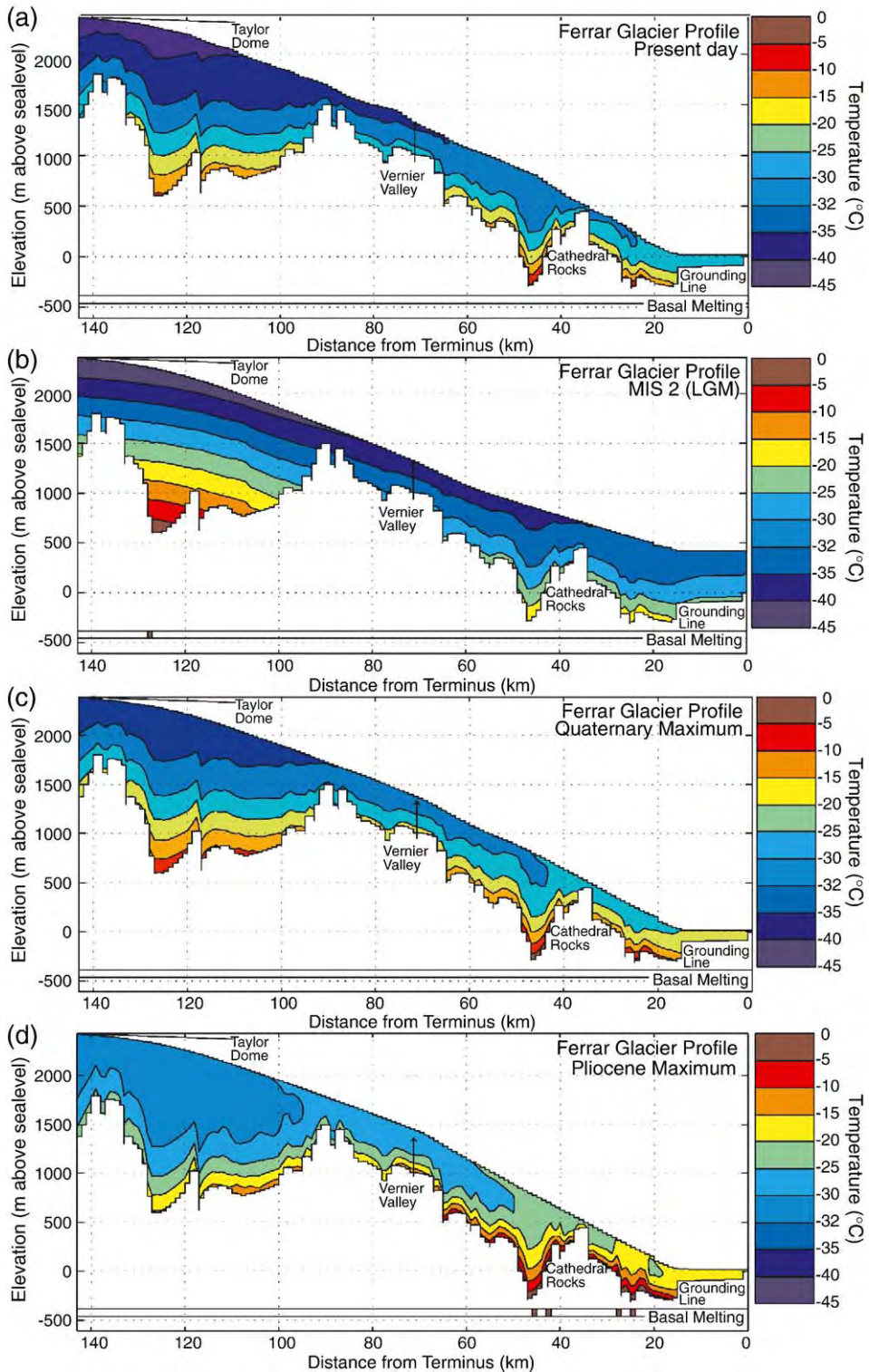
4.2.3. Upper Ferrar Glacier during the Pliocene Climatic Optimum

Regardless of the precise erosion rate used to calculate drift ages (0 cm , 5 cm , or 10 cm Ma^{-1} , Table 2), our data show that during the Pliocene Climatic Optimum (PCO; centered around 3–4 Ma) the ice-surface elevation of upper Ferrar Glacier was higher than at present, not lower as some have implied [9]. Using our preferred age model that incorporates a very conservative erosion rate of 5 cm Ma^{-1} , we show that between ~ 4 Ma and ~ 1 Ma, the margin of Ferrar Glacier stood ~ 100 – 120 m higher than at present (Tables 1 and 2). This finding of a thicker-than-present Ferrar Glacier during the PCO is consistent with results from numerical, 3-D ice sheet models that call for ice sheet expansion with modest atmospheric warming $\leq 5 \text{ }^\circ\text{C}$ [44] and with glacial-geologic data from nearby Arena Valley. For example, based on the calculated He-3 cosmogenic ages on boulders deposited from Taylor Glacier in Arena Valley (10 km northwest of Vernier Valley, Fig. 1), [1,16,26,41] demonstrated that between ~ 2.2 and $\geq \sim 3.5$ Ma, the ice-surface elevation of Taylor Glacier stood ~ 200 – 300 m above present values (values based on the reported age and elevation of Taylor IVb and Quartermain I drifts in Arena Valley). Likewise, glacial-geologic data from central Taylor Valley [43] suggest a thicker-than-present Taylor Glacier at ~ 3.0 Ma. A greater rate of snowfall during the Pliocene Climatic Optimum (analogous to an increase in snowfall during the Holocene, see below) is commonly cited as one explanation for advance during this time [43,44].

Lastly, we note that our overall conclusion for modest fluctuations in the volume of East Antarctic

ice during the last ~4 Ma is consistent with glacial-geologic and cosmogenic data from the Beardmore Glacier region (central Transantarctic Mountains)

that show <130 m change in the surface elevation of the Beardmore glacier during Plio-Pleistocene time [40].



4.2.4. Upper Ferrar Glacier during marine-oxygen isotope stage 2 (MIS 2)

MIS 2 represents the last global ice-age maximum as recorded in deep-sea cores. Vernier Valley apparently lacks drift deposited from Ferrar Glacier dating to this time. One possible explanation is that such drift *did* form, but that the modern Ferrar Glacier at the valley mouth now covers it. If so, the implication would be that during MIS 2 the ice-surface elevation of upper Ferrar Glacier was lower than present. This inference is consistent with the measured Holocene (MIS 1) advance of outlet glaciers draining Taylor Dome (see also [3,16]). Also, records of ice accumulation at Taylor Dome show that during MIS 2 annual snowfall yielded <1 mm ice equivalent yr^{-1} , whereas annual snowfall now yields ~ 70 mm ice equivalent yr^{-1} [12,13].

In sharp contrast with the dynamics of upper Ferrar Glacier, the ice-surface elevation of lower Ferrar Glacier actually rose by ~ 400 m during MIS 2 [45]. The increase in ice-surface elevation near the glacier mouth resulted from blocked ice flow. Grounded glacier ice occupied McMurdo Sound, advancing westward into Ferrar Glacier valley between $\sim 23,840$ ^{14}C yr BP to ~ 8340 ^{14}C yr BP, causing ice to back up near the mouth of Ferrar Glacier valley [46].

4.3. Modeling the basal thermal regime of Ferrar Glacier

We modeled the basal thermal regime for the modern Ferrar Glacier and for ancestral Ferrar Glaciers during what we believe to be MIS 2, the Quaternary maximum, and the PCO (Fig. 7). Model specifications and input parameters are detailed in the online supplement.

The striking results of these simulations are that even during the dramatic atmospheric warming purported for the PCO (modeled here with local atmospheric temperatures 10 °C above present values), basal melting is limited and only occurs in a few locations seaward of Vernier Valley (Fig. 7). The implication is that ice temperatures along the base of the Ferrar Glacier inland of Vernier Valley likely remained below the pressure-melting point for at least the last ~ 4 Ma.

4.4. Paleoclimate reconstruction from textural characteristics of Ferrar drifts

The texture of Ferrar 2, 3, and 4 drifts are identical to that of Ferrar 1 at the margin of the modern Ferrar Glacier. This textural similarity, along with the preservation of undisturbed colluvium and till beneath Ferrar 3 and 4 drifts, is consistent with our modeling studies and indicates that all Ferrar drifts were likely deposited from frozen-based ice. The presence of thin lobes (≤ 125 m thick) of frozen-based ice for the last ~ 4 Ma at the mouth of Vernier Valley imply persistent cold-desert conditions, much like those of today.

In addition, the remarkable absence of outwash sediments, lacustrine deposits, ice-marginal channels, kame terraces, or other glacio-fluvial/waterlain sediment in lower Vernier Valley indicates that here lobes of Ferrar Glacier ice did not develop surface-melting ablation zones. Because such zones develop only on glaciers that occur near the 0 °C atmospheric isotherm, we argue that mean annual temperatures in the Wilkniss Mountains remained below 0 °C over the last ~ 4 Ma. Lastly, the presence of in situ moraine ridges on steep valley walls ($\sim 28^\circ$ on the west wall of lower Vernier Valley, Fig. 3d) implies little slope development for the last ~ 4 Ma. Otherwise, moraine ridges and drifts would be eroded or buried beneath younger colluvial deposits. Such stability is best explained by persistent cold-desert conditions similar to the present.

5. Conclusions

The areal distribution of Ferrar drifts in lower Vernier Valley, along with a relative and numerical chronology afforded by surface-weathering characteristics and ^{21}Ne exposure-age data, imply progressive thinning of a peripheral lobe of Ferrar Glacier in Vernier Valley over the last ~ 4 Ma. Upper Ferrar Glacier stood ~ 100 to ~ 125 m higher than present during the Pliocene Climatic Optimum and most likely ~ 50 m higher during early- to mid-Quaternary time. The ice-surface elevation of upper Ferrar Glacier may have been lower-

Fig. 7. Modeled temperature fields for Ferrar Glacier at (a) present time, (b) Last Glacial Maximum (MIS 2), (c) inferred Quaternary maximum, and (d) inferred Pliocene Climatic Optimum. For MIS 2, the following parameters (deviating from today's values) were used as input to our glaciological model (online supplement): a reduction in atmospheric temperature of 3 °C; an increase by a factor of two for the accumulation lapse rate; an increase in the ice-surface elevation at the grounding line of Ferrar Glacier of ~ 400 m (e.g., [34]). Parameters for the inferred Quaternary maximum include an increase in atmospheric temperature of 3 °C and an integrated increase in ice-surface elevation of Ferrar Glacier equal to $+50$ m near Vernier Valley. For the inferred Pliocene Climatic Optimum, parameters included an atmospheric temperature increase of 10 °C, an increase in accumulation lapse rates by a factor of 2, and an integrated increase in ice-surface elevation of Ferrar Glacier equal to $+125$ m near Vernier Valley. Temperatures computed in steady state from the model of Hooke [24]. All figures share a common temperature range; thus, not all colors appear in all figures. See online supplement for additional details.

than-present during MIS 2. This lowering most likely reflects reduced precipitation at Taylor Dome.

Numerical models that calculate basal–thermal conditions for upper Ferrar Glacier, as well as our measured textural and sedimentological data for Ferrar drifts, show that basal- and near-surface ice remained below the melting point during deposition of all Ferrar drifts. Our numerical-modeling shows that Ferrar Glacier cannot achieve a fully melted bed even with a modeled atmospheric temperature increase of 10 °C.

We find near-linear relationships among drift age, surface-weathering pits, and the maximum thickness of desert varnish for cobbles exposed atop Ferrar drifts. Our calculated rates of $\sim 6.7 \text{ mm Ma}^{-1}$ and $\sim 10 \text{ mm Ma}^{-1}$ for the deepening and widening of surface pits, as well as our measured increase in maximum thickness of desert varnish of $\sim 1.5 \text{ mm Ma}^{-1}$ on exposed dolerite cobbles, may be used to help calibrate the age of dolerite-rich drifts with similarly pitted and varnished surface cobbles elsewhere in the western Dry Valleys region.

Acknowledgements

The authors are indebted to Dr. Ken Tonka, Brett VandenHeuvel, Sarah Burns, and Emily Klingler for excellent assistance in the field. We also thank Terry Plank, Linda Farr and Katie Kelley for assistance with LA–ICP–MS analyses. Funding was provided by NSF OPP Grants 9811877 and 0338291 to DRM. JMS would like to thank the CSEF and the L-DEO Climate Center for their support. Lastly, we remember the excellent contributions to Antarctic science made by Dr. Peter E. Wilkniss (1934–2005), for whom the Wilkniss Mountains are so named.

Appendix A. Supplementary data

Supplementary data associated with this article can be found, in the online version, at [doi:10.1016/j.epsl.2006.01.037](https://doi.org/10.1016/j.epsl.2006.01.037).

References

- [1] D.R. Marchant, G.H. Denton, C.C. Swisher III, Miocene–Pliocene–Pleistocene glacial history of Arena Valley, Quaternary Mountains, Antarctica, *Geogr. Ann.* 75A (1993) 269–302.
- [2] D.R. Marchant, G.H. Denton, D.E. Sugden, C.C. Swisher III, Miocene glacial stratigraphy and landscape evolution of the western Asgard Range, Antarctica, *Geogr. Ann.* 75A (1993) 303–330.
- [3] G.H. Denton, D.E. Sugden, D.R. Marchant, B.L. Hall, T.I. Wilch, East Antarctic Ice Sheet sensitivity to Pliocene climate change from a Dry Valleys perspective, *Geogr. Ann.* 75A (1993) 155–204.
- [4] G.H. Denton, T.J. Hughes, Potential influence of floating ice shelves on the climate of an ice age, *S. Afr. J. Sci.* 82 (1986) 509–513.
- [5] G.H. Denton, D.E. Sugden, Meltwater features that suggest Miocene ice-sheet over-riding of the Transantarctic Mountains in Victoria Land, Antarctica, *Geogr. Ann.* 87A (2005) 67–85.
- [6] K.G. Miller, J.D. Wright, R.G. Fairbanks, Unlocking the Ice House: Oligocene–Miocene oxygen isotopes, eustasy, and margin erosion, *J. Geophys. Res.* 96 (1991) 6829–6848.
- [7] J.C. Zachos, M. Pagani, L. Stone, E. Thomas, K. Billups, Trends, rhythms, and aberrations in global climates 65 Ma to present, *Science* 292 (2001) 293–686.
- [8] T.R. Naish, K.J. Woolfe, P.J. Barrett, G.S. Wilson, C. Atkins, S.M. Bohaty, C.J. Becker, M. Claps, F.J. Davey, G.B. Dunbar, A.G. Dunn, C.R. Fielding, F. Florindo, M.J. Hannah, D.M. Harwood, S.A. Henerys, L.A. Krissek, M. Lavelle, J. Van Der Meer, W.C. McIntosh, F. Niessen, S. Passchier, R.D. Powell, A.P. Roberts, L. Sagnotti, R.P. Scherer, C.P. Strong, F. Talarico, K.L. Verosub, G. Villa, D.K. Watkins, P.N. Webb, T. Wonik, Orbital induced oscillations in the East Antarctic ice sheet at the Oligocene/Miocene boundary, *Nature* 413 (2001) 719–723.
- [9] P.N. Webb, D.M. Harwood, Late Cenozoic glacial history of the Ross Embayment, Antarctica, *Quat. Sci. Rev.* 10 (1991) 215–223.
- [10] K. Billups, D.P. Schrag, Paleotemperatures and ice volume of the past 27 Myr revisited with paired Mg/Ca and $^{18}\text{O}/^{16}\text{O}$ measurements on benthic foraminifera, *Paleoceanography* 17 (2002) 1–11.
- [11] J. Huybrechts, I. Gregory, M. Janssens, Modelling Antarctic and Greenland volume changes during the 20th and 21st centuries forced by GCM time slice integrations, *Glob. Planet. Change* 42 (2004) 83–105.
- [12] D.L. Morse, E.D. Waddington, E.J. Steig, Ice age storm trajectories inferred from radar stratigraphy at Taylor Dome, Antarctica, *Geophys. Res. Lett.* 25 (1998) 3383–3386.
- [13] E.J. Steig, E.J. Brook, J.W.C. White, C.M. Sucher, M.L. Bender, S.J. Lehman, D.L. Morse, E.D. Waddington, G.D. Clow, Synchronous climate changes in Antarctica and the North Atlantic, *Science* 281 (1998) 92–95.
- [14] D.J. Drewry, Ice flow, bedrock, and geothermal studies from radio-echo sounding inland of McMurdo Sound, Antarctica, Antarctic Geoscience, International Union of Geological Sciences, 1982, pp. 977–983.
- [15] P.H. Robinson, Ice dynamics and thermal regime of Taylor Glacier, South Victoria Land, Antarctica, *J. Glaciol.* 30 (1984) 153–160.
- [16] D.R. Marchant, G.H. Denton, J.G. Bockheim, S.C. Wilson, A.R. Kerr, Quaternary changes in level of the upper Taylor Glacier, Antarctica: implications for paleoclimate and East Antarctic Ice Sheet dynamics, *Boreas* 23 (1994) 29–43.
- [17] H. Baur, A noble-gas mass spectrometer compressor source with two orders of magnitude improvement in sensitivity, *AGU*, vol. 80, 1999, p. 1118.
- [18] J.M. Schäfer, S. Ivy-Ochs, R. Wieler, I. Leya, H. Baur, G.H. Denton, C. Schlüchter, Cosmogenic noble gas studies in the oldest landscape on earth: surface exposure ages of the Dry Valleys, Antarctica, *Earth Planet. Sci. Lett.* 167 (1999) 215–226.

- [19] T.E. Cerling, H. Craig, Geomorphology and in-situ cosmogenic isotopes, *Annu. Rev. Earth Planet. Sci.* 22 (1994) 273–317.
- [20] S. Niedermann, The ^{21}Ne production rate in quartz revisited, *Earth Planet. Sci. Lett.* 183 (2000) 361–364.
- [21] F. Kober, S. Ivy-Ochs, I. Leya, H. Baur, T. Magna, R. Wieler, P. W. Kubik, In situ cosmogenic ^{10}Be and ^{21}Ne in sanidine and in situ cosmogenic ^3He in FeTi-oxide minerals, *Earth Planet. Sci. Lett.* 236 (2005) 404–418.
- [22] J.O. Stone, Air pressure and cosmogenic isotope production, *J. Geophys. Res.* 105 (2000) 23753–23759.
- [23] W. Paterson, *The Physics of Glaciers*, Pergamon, Oxford, 1994.
- [24] R.L. Hooke, *Principles of Glacier Mechanics*, Prentice Hall, Upper Saddle River, NJ, 1998.
- [25] W. Budd, D. Jenesen, U. Radok, Derived physical characteristics of the Antarctic Ice Sheet, Australian National Antarctic Expeditions Interim Report, Series A(IV), *Glaciology* 108 (1971).
- [26] E.J. Brook, M.D. Kurz, R.P. Ackert Jr., G.H. Denton, E.T. Brown, G.M. Raisbeck, F. Yiou, Chronology of Taylor Glacier advances in Arena Valley, Antarctica, using in situ cosmogenic ^3He and ^{10}Be , *Quat. Res.* 39 (1993) 11–23.
- [27] K. Willenbring, History of the Ferrar Glacier, Dry Valleys, Antarctica: implications for climate and ice sheet stability, Masters Thesis, Boston University, Boston, Massachusetts, 1–153 pp.
- [28] D.R. Marchant, G.H. Denton, Miocene and Pliocene paleoclimate of the Dry Valleys region, Southern Victoria Land: a geomorphological approach, *Mar. Micropaleontol.* 27 (1996) 253–271.
- [29] D.R. Marchant, G.H. Denton, C.C. Swisher III, N. Potter Jr., Late Cenozoic Antarctic paleoclimate reconstructed from volcanic ashes in the Dry Valleys region, south Victoria Land, *Geol. Soc. Amer. Bull.* 108 (1996) 181–194.
- [30] D.E. Sugden, D.R. Marchant, N. Potter Jr., R. Souchez, G.H. Denton, C.C. Swisher III, J.-L. Tison, Miocene glacier ice in Beacon Valley, Antarctica, *Nature* 376 (1995) 412–416.
- [31] D.R. Marchant, A.R. Lewis, W.C. Phillips, E.J. Moore, R. Souchez, G.P. Landis, Formation of patterned-ground and sublimation till over Miocene glacier ice in Beacon Valley, Antarctica, *Geol. Soc. Amer. Bull.* 114 (2002) 718–730.
- [32] R. Parsons, J.W. Head III, D.R. Marchant, Weathering pits in the Antarctic Dry Valleys: insolation-induced heating and melting, and applications to Mars, *Lunar Planet. Sci. Conf.*, vol. 36, 2005, Abstract #1776.
- [33] R. Weed, R.P. Ackert Jr., Chemical weathering of Beacon Supergroup sandstones and implications for Antarctic glacial chronology, *S. Afr. J. Sci.* 82 (1986) 513–516.
- [34] R. Weed, S.A. Norton, Siliceous crusts, quartz rinds and biotic weathering of sandstones in the cold desert of Antarctica, in: J. Berthelin (Ed.), *Proceedings of the International Symposium of Environmental Biogeochemistry*, Nancy, France, 1991, pp. 327–340.
- [35] L.A. Bruno, H. Baur, T. Graf, C. Schluchter, P. Singer, R. Wieler, Dating of Sirius Group tillites in the Antarctic Dry Valleys with cosmogenic ^3He and ^{21}Ne , *Earth Planet. Sci. Lett.* 147 (1997) 37–54.
- [36] P. Oberholzer, C. Baroni, J.M. Schaefer, G. Orombelli, S. Ivy-Ochs, P.W. Kubik, H. Baur, R. Wieler, Limited Pliocene/Pleistocene glaciation in Deep Freeze Range, northern Victoria Land, Antarctica, derived from in-situ cosmogenic nuclides, *Antarct. Sci.* 15 (2003) 493–502.
- [37] J.M. Schaefer, D.R. Marchant, G.H. Denton, R. Wieler, S. Ivy-Ochs, C. Schluchter, The oldest ice on Earth in Beacon Valley, Antarctica: new evidence from surface exposure dating, *Earth Planet. Sci. Lett.* 179 (2000) 91–99.
- [38] P. Oberholzer, Reconstructing paleoclimate and landscape history in Antarctica and Tibet with cosmogenic nuclides, PhD dissertation, ETH Zurich, 2004.
- [39] M.A. Summerfield, F.M. Stuart, H.A.P. Cockburn, D.E. Sugden, G.H. Denton, T. Dunai, D.R. Marchant, Long-term rates of denudation in the Dry Valleys, Transantarctic Mountains, southern Victoria Land, Antarctica based on in-situ-produced cosmogenic ^{21}Ne , *Geomorphology* 27 (1999) 113–129.
- [40] R.P. Ackert Jr., M.D. Kurz, Age and uplift rates of Sirius Group sediments in the Dominion Range Antarctica, from surface exposure dating and geomorphology, *Glob. Planet. Change* 42 (2004) 207–225.
- [41] E.J. Brook, E.T. Brown, M.D. Kurz, R.P. Ackert Jr., G.M. Raisbeck, F. Yiou, Constraints on age, erosion, and uplift of Neogene glacial deposits in the Transantarctic Mountains determined from in-situ cosmogenic ^{10}Be and ^{21}Al , *Geology* 23 (1995) 1063–1066.
- [42] H.R. Margerison, W.M. Phillips, F.M. Stuart, Cosmogenic He-3 concentrations in ancient flood deposits from the Coombs Hills, northern Dry Valleys, East Antarctica: interpreting exposure ages and erosion rates, *Earth Planet. Sci. Lett.* 230 (2005) 163–175.
- [43] T.I. Wilch, G.H. Denton, D.R. Lux, W.C. McIntosh, Limited Pliocene glacier extent and surface uplift in Middle Taylor Valley, *Geogr. Ann.* 75A (1993) 331–351.
- [44] R.C.A. Hindmarsh, Modeling the dynamics of ice sheets, *Prog. Phys. Geogr.* 17 (1993) 391–412.
- [45] G.H. Denton, D.R. Marchant, The geologic basis for a reconstruction of a grounded ice sheet in McMurdo Sound, Antarctica, at the last glacial maximum, *Geogr. Ann.* 82A (2000) 167–211.
- [46] B.L. Hall, G.H. Denton, Radiocarbon chronology of Ross Sea Drift, Eastern Taylor Valley, Antarctica: evidence for a grounded ice sheet in the Ross Sea at the last glacial maximum, *Geogr. Ann.* 82A (2000) 305.
- [47] T.E. Cerling, H. Craig, Cosmogenic ^3He production rates from 39degN to 46degN latitude, western USA and France, *Geochim. Cosmochim. Acta* 58 (1994) 249–255.